Highly Effective Scaling Mitigation in Membrane Distillation using Superhydrophobic Membrane with Gas Purging

Environmental Science & Technology Letters

Authors: Thomas Horsemant, Chunlei Suts, Kofi S. S. Christies, Shihong Lints

† Department of Chemical and Biomolecular Engineering, Vanderbilt University, Nashville, USA 37235 † University of Chinese Academy of Sciences, Beijing, China, 100190 § Department of Civil and Environmental Engineering, Vanderbilt University, Nashville, USA 37235

Corresponding author: email: shihong.lin@vanderbilt.edu; Tel. +1(615)322-7226

1 Abstract

2

3

4 5

6 7

8

9

10

11

12

13

14

15

16 17

18

Membrane distillation (MD) is a thermal desalination process with the capability of harnessing low-grade waste heat to treat hypersaline brine. For this reason, MD has been actively explored as a promising technology for brine management and zero-liquid discharge (ZLD). The major and inevitable challenge with conventional hydrophobic MD membranes, however, is membrane scaling, i.e., the formation and deposition of mineral crystal on the membrane surface which eventually leads to process failure. By performing comparative MD experiments in this study, we show that superhydrophobic membrane or gas purging can slightly alleviate gypsum scaling, but neither of them is an effective strategy to achieve sustained MD performance against gypsum scaling. However, the synnergistic combination of both superhydrophobic membrane and periodic gas purging is extraordinarily effective in mitigating gypsum scaling in MD, enabling the MD process to concentrate a highly saline feed stream by five-fold without suffering flux decline due to scaling that is always observed with commercial hydrophobic membrane. Energy dispersive X-ray spectroscopy (EDS) reveals the formation of crystal "anchors" inside the pores of the commercial hydrophobic membranes but not those of the superhydrophobic membrane, which explains the different effectivenesses of purging in mitigating scaling for the two membranes. The long term flux stability offered with this scaling mitigation scheme is important for MD to be applied for brine management and ZLD.

Introduction

Membrane distillation (MD) is a thermal desalination process in which water evaporation and condensation occurs within the pores of a microporous hydrophobic membrane1. As a desalination process that can harness low-grade waste heat to treat hypersaline brine, MD has been actively explored as a promising technology for brine management in produced water treatment and zero liquid discharge (ZLD)₂₋₆. Managing hypersaline brine is a critical environmental challenge, especially because reverse osmosis (RO), the state-of-the-art desalination technology, cannot be applied in these scenarios where the brine osmotic pressure exceeds the current allowable working pressure of RO₇₋₁₀. In comparison, the performance of MD as a thermal distillation process is relatively independent of brine salinity, which in theory allows MD to achieve a high degree of brine volume reduction or even brine crystallization_{11,12}. The major and inevitable challenge toward such an application, however, is membrane scaling, i.e., the formation or deposition of mineral crystal on the membrane surface that ultimately leads to complete process failure_{1,4}.

Scaling is detrimental to MD performance because crystals may (1) block membrane pores, which reduces membrane permeability for vapor transfer, and (2) grow through the pores, allowing salty feed solution to pass directly through the membrane and contaminate the distillate (i.e. wetting)₁₃. The mode of crystal growth during scaling is mixed. Some crystals nucleate homogeneously or heterogeneously from seeds in the bulk solution and deposit onto the membrane surface, while other crystals may nucleate heterogeneously directly on the membrane surface and grow in-situ (i.e. interfacial crystallization)_{14,15}. Interfacial crystallization is more problematic because it may lead to larger contact area and thus stronger overall crystal-polymer interaction_{16,17}. This also allows crystals to mold to the geometry of the membrane pore structure and further enhance the crystal-membrane interaction. In contrast, large crystals that form in the

bulk solution and deposit onto the membrane surface have weaker interaction and smaller areal contact with the membrane surface₁₈.

Classical nucleation theory suggests that heterogeneous crystallization on surfaces with the right interfacial properties is favored over homogeneous crystallization 19. With that, increasing membrane hydrophobicity has been shown to discourage interfacial crystallization and reduce the overall scaling kinetics20-25. However, only delaying scaling is insufficient for practical application of MD in treating hypersaline brine if scaling is irreversible. Previous MD studies have also investigated gas purging, or blowing compressed air through the membrane pores from the distillate to the feed side, for scale mitigation26,27. These studies show that purging was only effective when the initial feed concentration was well above saturation so that most of the crystals formed in the bulk solution and deposited on the membrane surface. With the initial feed concentration below saturation, mineral crystals form within the membrane pores and become "anchor points" for the scale layer, which significantly compromises the effectiveness of purging21.

With conventional hydrophobic membranes, feed solution partially intrudes into the membrane pores, as the hydraulic pressure of the circulating feed stream exceeds the liquid entry pressure of some pores near the membrane surface21,22,25. Such partial intrusion increases the solid-water contact area available for interfacial heterogeneous crystallization and promotes the in-pore formation of mineral crystal "anchors" that lead to a robust scale layer that cannot be removed by purging (Figure 1A). We hypothesize that the use of superhydrophobic membrane, which significantly reduces solid-water contact, will minimize in-pore crystal formation and the adhesion of crystal to the membrane surface, thereby making purging significantly more effective in maintaining membrane performance by removing the deposited salt crystals (Figure 1B).

(A) Hydrophobic Membrane (B) Superhydrophobic membrane in-pore crystallization (anchoring) purging ineffective purging effective

Figure 1: Schematic illustration of the central hypothesis in this study. (A) with a conventional hydrophobic membrane, feed solution partially wets the pores near the membrane surface, resulting in in-pore growth of gypsum crystals. Consequently, gas purging is ineffective in removing the crystal due to stronger adhesion and physical anchoring. (B) with a superhydrophobic membrane, intrusion of feed solution and thus in-pore growth of crystal are minimized, which renders gas purging highly effective in removing the crystal deposited on the membrane surface.

In this study, we test the above hypothesis by comparing the effectiveness of purging in maintaining the performance of hydrophobic and superhydrophobic membranes subject to gypsum scaling. We first fabricate a superhydrophobic membrane by modifying the surface of a commercial polyvinylidene fluoride (PVDF) membrane using silica nanoparticles (SiNPs) coated with fluoroalkylsilane (FAS). We then perform MD experiments using the hydrophobic and superhydrophobic membranes with under-saturated gypsum feed solution to compare the scaling kinetics and scale morphology with and without periodic purging. Finally, we also examine the morphology of scaled membrane to elucidate the difference in the effectiveness between different scaling mitgation strategies.

Materials and Methods

Materials and Chemicals. The commercial hydrophobic PVDF membrane with 0.45 μm nominal pore size was purchased from GE Healthcare (Pittsburg, PA). Sodium hydroxide (NaOH), 200 proof ethanol, 3-aminopropyl-triethoxysilane (APTES, 99%), trizma-hydrochloride buffer,

LUDOX HS-40 colloidal silica (SiNPs) with a diameter of 12 nm, hydrochloric acid (HCl), calcium chloride (CaCl₂), sodium sulfate (Na₂SO₄), and 1H, 1H, 2H, 2H-perfluorodecyltriethoxysilane (fluoroalkylsilane, or FAS, 97%) were purchased from Sigma Aldrich (St. Louis, MO). Silica nanoparticles (SiNPs) with a diameter of 40-60 nm were purchased from SkySpring Nanomaterials (Houston, TX).

88

89

90

91

92

93

94

95

96

97

98

99

100

101

102

103

104

105

106

107

108

109

110

111

112

113

Fabrication of Superhydrophobic Membrane. The superhydrophobic membrane was obtained by modifying the commercial PVDF membrane using FAS-coated SiNPs similar to the approach reported by Boo et al.28. First, a pristine commercial PVDF membrane surface was placed on 7.5 M NaOH solution for 3-4 hrs at 70°C. Due to the hydrophobicity, the PVDF membrane floated on the solution, which chemically modified only the membrane surface in contact with the NaOH solution to generate an abundance of surface hydroxyl groups. The treated membrane was then rinsed thoroughly with DI water and dried for 1.5 hrs at 70°C. The membrane surface was then immersed in 1 vol% APTES (in ethanol) for 1 hr under gentle mixing. SiNPs with a diameter of 40-60 nm were then dispersed at 1 wt% in 10 mM trizma hydrochloride with the pH adjusted to 4 at which point the APTES-functionalized surface is positively charged and the SiNPs are negatively charged. The APTES-functionalized surface of the PVDF membrane was placed in contact with the SiNPs dispersion for SiNPs adsorption onto the surface via electrostatic interaction. As only the surface of the membrane was functionalized, the bulk of the membrane maintained its hydrophobicity and thus floated on the SiNPs dispersion, adding SiNPs only to the surface. The SiNPs-coated surface was rinsed with DI water and dried. Such functionalization and adsorption process was repeated with 12 nm diameter SiNPs (i.e. applying the exact same procedure to the PVDF membrane coated with SiNPs of 40-60 nm diameter). Finally, the SiNPcoated membrane surface was silanized with FAS via vapor phase reaction at 80°C overnight. The surface modification process is schematically illustrated in Figure S1.

Membrane Characterization. We compared the surface wetting properties of the membranes by measuring the static water contact angle (CA) with an optical tensiometer (T114,

Attension, Finland). We also quantified the CA hysteresis by measuring the sliding angle (SA) which is the critical tilting angle at which a water droplet starts to slide. The membrane surface morphology was characterized with scanning electron microscopy (SEM, Zeiss Merlin).

Membrane Scale Purging Experiments. We used a direct contact MD system to perform the MD scaling experiments with feed inlet temperature maintained at 75°. The distillate inlet temperatures for MD experiments using the superhydrophobic and hydrophobic membranes were set at 18°C and 43°C, respectively, to maintain a constant flux of 25 L m-2 h-1 in all cases and thus maintain the same level of concentration polarization (CP). The flow rates of the feed and distillate were maintained at 600 mL min-1 and 500 mL min-1 (12.8 and 10.7 cm s-1 in our MD module), respectively. The feed mixture, with initial volume of 500 mL, contained 14 mM CaCl₂ and 14 mM Na₂SO₄. At 75°C, the gypsum saturation index, defined as the natural log of the ion activity product over the solubility product, was -0.10 (PHREEQC version 3.0 from the USGS)₂₉. The distillate mass and conductivity were recorded real-time to determine water vapor flux and salt rejection.

During the purging steps, we first drained the distillate side of the MD cell, closed its exit, and filled it with compressed nitrogen at 60 kPa. These operations on the distillate side were performed without interrupting the feed stream. The purging was performed for 60s every hour. Experiments were terminated when the remaining feed volume was approximately 100 mL, or concentrated roughly by a factor of five, and became insufficient to keep the feed loop free of air bubbles. A detailed schematic of the scale purging set up is presented in the supporting information (Figure S2).

Results and Discussion

Membrane Surface Properties. The adsorption of SiNPs onto the commercial PVDF membrane surface significantly enhances the surface roughness which is indispensible for achieving superhydrophobicity. The change of surface morphology is confirmed by comparing the

SEM images of the PVDF membrane (Figure 2A) and the superhydrophobic membrane (Figure 2B). Due to both the high surface roughness and the low surface energy of the FAS coating, a very high water CA of $166 \pm 4^{\circ}$ was measured with the superhydrophobic membrane (inset of Figure 2B) as compared to the water CA of $115 \pm 9^{\circ}$ measured with the hydrophobic membrane (inset of Figure 2A).

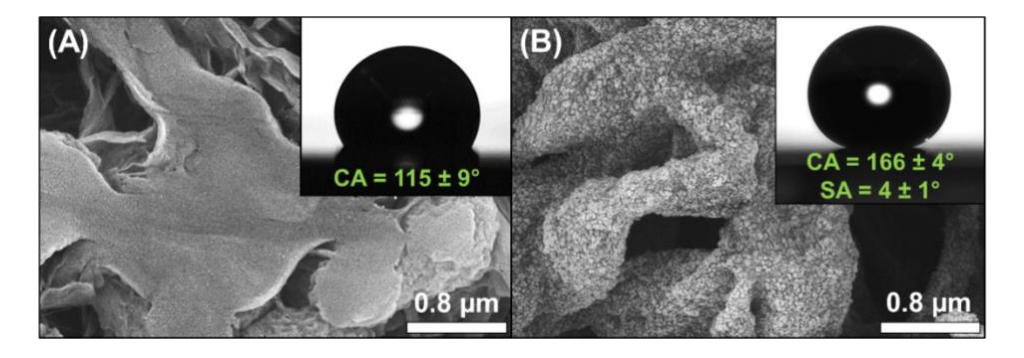


Figure 2: SEM images of (A) commercial hydrophobic and (B) superhydrophobic membranes. Inset images show static water contact angle (CA) and sliding angle (SA) measured with 10 μ L DI water droplets. The SA of the commercial hydrophobic PVDF membrane is not reported as it was not measureable, i.e. the drop remained pinned even with an inverted membrane surface.

The superhydrophobic membrane also yields an extremely low CA hysteresis. Compared to the very strong CA hysteresis of a commercial PVDF membrane with an unmeasurable SA (i.e. the water droplet remained adhered to an inverted membrane surface), the SA for the superhydrophobic membrane is only $4 \pm 1^{\circ}$. Using a mixture of SiNPs of two different sizes (40-60 nm and 12 nm) as the morphological modifier works signifcantly better than using single-sized SiNPs (40-60 nm) for imparting the superhydrophobicity. When single-sized SiNPs were used as the sole morphological modifier, the CA was only $148 \pm 2^{\circ}$ (as compared to $166 \pm 4^{\circ}$) and the SA was higher than 20° (as compared to $4 \pm 1^{\circ}$). The superior superhydrophobicity obtained using SiNPs of two different sizes may be attributed to the better surface coverage and/or to the hierarchical texture_{30,31}. Regardless of the mechanism, the membrane modified with SiNPs of two different sizes achieves the superhydrophobicity (both ultrahigh CA and ultralow SA) that is

required for testing our hypothesis. The excellent Cassie-Baxter state maintains a stable air layer near the membrane surface that helps to mitigate interfacial crystallization₁₃. It also minimizes the depth of feed solution intrusion and the consequent growth of crystals within the membrane pores₂₁.

Membrane Scaling and Effect of Purging. The scaling behaviors of the hydrophobic and superhydrophobic membranes were first compared without purging. As more water was recovered, the feed solution became increasingly concentrated and eventually supersaturated. Formation of gypsum crystal blocks membrane pores and causes significant flux declines. Apparent flux decline occurs at a limiting saturation level, or equivalently, a limiting cummulative water recovery. This limiting recovery was around 250 mL for both the hydrophobic and superhydrophobic membranes (Figure 3A). Furthermore, the initial scaling rates, defined as the average drop of normalized vapor flux per increment of distillate volume after scaling starts (i.e. the slope of flux decline in Figure 3A, which has a dimension of volume-1), also differ between the two membranes. Before the occurance of membrane wetting, indicated by the sharp increase in distillate conductivity at 325 mL for both membranes (Figure S3A), the initial scaling rate was around -11 ± 1 L-1 for the hydrophobic membrane, as compared to around -7 ± 4 L-1 for the superhydrophobic membrane. These observations of reduced scaling kinetics with increased membrane hydrophobicity are consistent with results from recent studies 13,21,25.

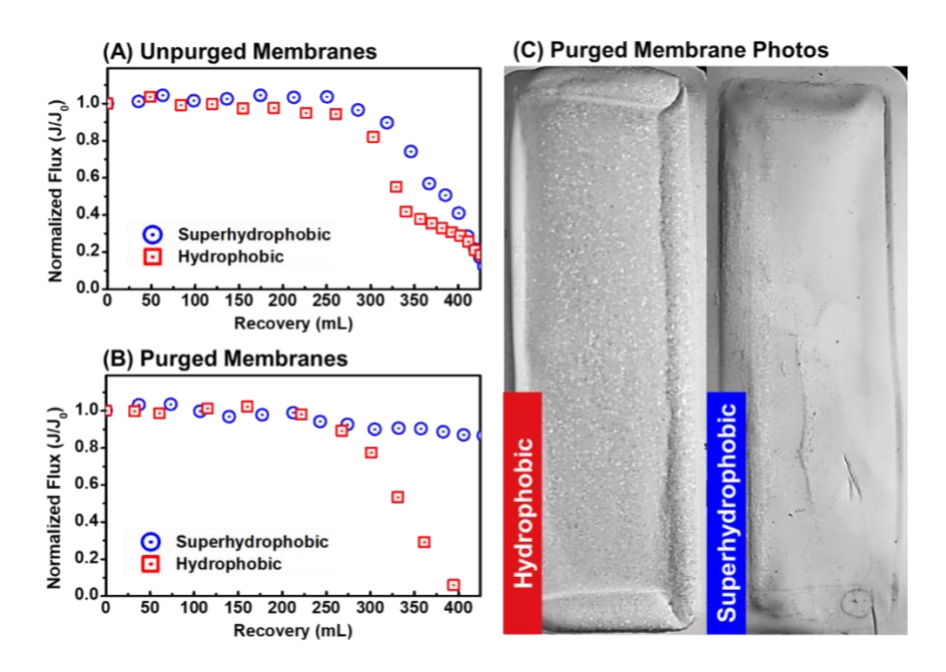


Figure 3: (A) Normalized water flux of the hydrophobic (red squares) and superhydrophobic (blue circles) membranes during MD operation without purging. (B) Normalized water flux of the hydrophobic (red squares) and superhydrophobic (blue circles) membranes during MD operation using periodic purging with 60kPa compressed N₂ for 60s per hour. The feed solution was 14 mM CaCl₂ and 14 mM Na₂SO₄ with an initial volume of 500 mL and the feed temperature was maintained at 75°C. The distillate temperatures in experiments with the superhydrophobic and hydrophobic membranes were maintained at 18 °C and 43 °C, respectively, such that the initial flux for both membranes was constant at 25 L m₋₂ h₋₁, which resulted in the same initial degree of concentration polarization. The flow rates of the feed and distillate were maintained at 600 mL min₋₁ and 500 mL min₋₁ (12.8 cm s₋₁ and 10.7 cm s₋₁ in our MD module), respectively. (C) Photographic images of hydrophobic (left) and superhydrophobic (right) membranes after MD scaling experiments with purging (corresponding to the results shown in B).

Delaying the initiation of membrane scaling or slowing scaling rate using superhydrophobic membrane is insufficient for practical applications of MD for treating hypersaline brine, because it does not address the fundamental challenge of scaling that leads to process failure. To truly enable MD for treating hypersaline brine, a strategy needs to be developed to either prevent scaling or readily recover the membrane performance after scaling occurs. Toward this goal, we implemented an operation scheme with periodic gas purging to physically remove the crystals deposited on the superhydrophobic membrane surface. With 60 seconds of N₂ gas purging every hour, scaling on superhydrophobic membrane was almost completely eliminated (blue circles in Figure 3B). Even though we observe a very small decline

of vapor flux, it is mostly attributable to the reduced partial vapor pressure driving force instead of the reduced permeability of the membrane due to pore blockage. The feed solution was concentrated by five folds at the end of the experiment, which signifcantly increased the salinity and reduced the partial vapor pressure of the feed solution at the same temperatures. Furthermore, the purged superhydrophobic membrane never wetted, indicated by stable near-zero distillate conductivity (Figure S3B).

204

205

206

207

208

209

210

211

212

213

214

215

216

217

218

219

220

221

222

223

224

225

226

227

228

229

In comparison, purging with the same operation scheme mitigates scaling on hydrophobic PVDF membrane to a significantly less extent. Compared to MD using hydrophobic membrane without purging, purging had negligible influence on detering scaling (Figure 3B): the the flux decline still occurred at ~250 mL of cumulative distillate volume and the rate of flux decline was also similar (-7 ± 3 L-1). However, wetting seemed to be delayed to ~350 mL with purging as compared to ~325 mL without purging (Figure S3). The appearance of the membrane surfaces after MD experiments (with purging, Figure 3C) differ dramatically between the hydrophobic and superhydrophobic membranes: there is clearly a film of crystal covering the entire surface of the hydrophobic membrane, whereas almost no crystal was observed on the superhydrophobic membrane except for a small fraction of the surface near the edge. Furthermore, the CA on the clear portions of the purged superhydrophobic membrane decreased very slightly to 160 ± 6° (compared to the original CA of 166 ± 4° before MD experiments). Such a CA was directly measured on the dried portion of the membrane after it was removed from the MD experiment without any further cleaning. This well-sustained superhydrophobicity suggests that (1) barely any gypsum crystal adhered onto surface of the superhydrophobic membrane when purging was implemented, and that (2) the FAS-coated SiNPs were stable even after multiple purging cycles.

Mechanism of Scale Mitigation via Purging. Heterogeneous nucleation on favorable surfaces usually occurs more readily (and thus faster) than homogeneous nucleation according to classical nucleation theory₁₉. Therefore, the increase of scaling kinetics by decreasing membrane hydrophobicity suggests that less hydrophobic surface is more favorable for

heterogeneous nucleation. The morphology of the crystal on the purged hydrophobic membrane (Figure 4A) reveals that the surface was almost fully covered by large rosette-like crystals, which is a common characteristic of heterogeneous nucleation in membrane desalination processes 33–35. Thus, purging was ineffective in scale removal from the hydrophobic membrane due to two possible reasons. The first is the stronger adhesion between the rosette-like crystals and the membrane surface due to both the higher surface energy of PVDF (than FAS on a superhydrophobic membrane) and the larger contact area. But perhaps more importantly, gypsum crystals grew within the hydrophobic membrane pores and formed crystal "anchors" that render physical removal of the scale layer very difficult (Figure 4B).

In contrast, purging the superhydrophobic membrane was effective in removing the crystals on the surface (Figure 4C). With superhydrophobic membranes, the crystals both on the unpurged membrane and the small fraction along one edge of the purged membrane (Figure 4C inset) were small, thin, and rod-like particles. The excellent Cassie-Baxter state achieved with the superhydrophobic membrane minimizes the intrusion of feed solution into the membrane pores and prevents the formation of crystal "anchors" within the membrane pores (Figure 4D). Therefore, periodic purging was effective in removing the deposited gypsum particles. We note that it is not possible to replicate this effect purely with improved hydrodynamics, e.g. by increasing the feed flow rate. A recent study shows that increased feed cross-flow velocity only delays, but does not prevent, mineral scaling on superhydrophobic membranes₂₁.

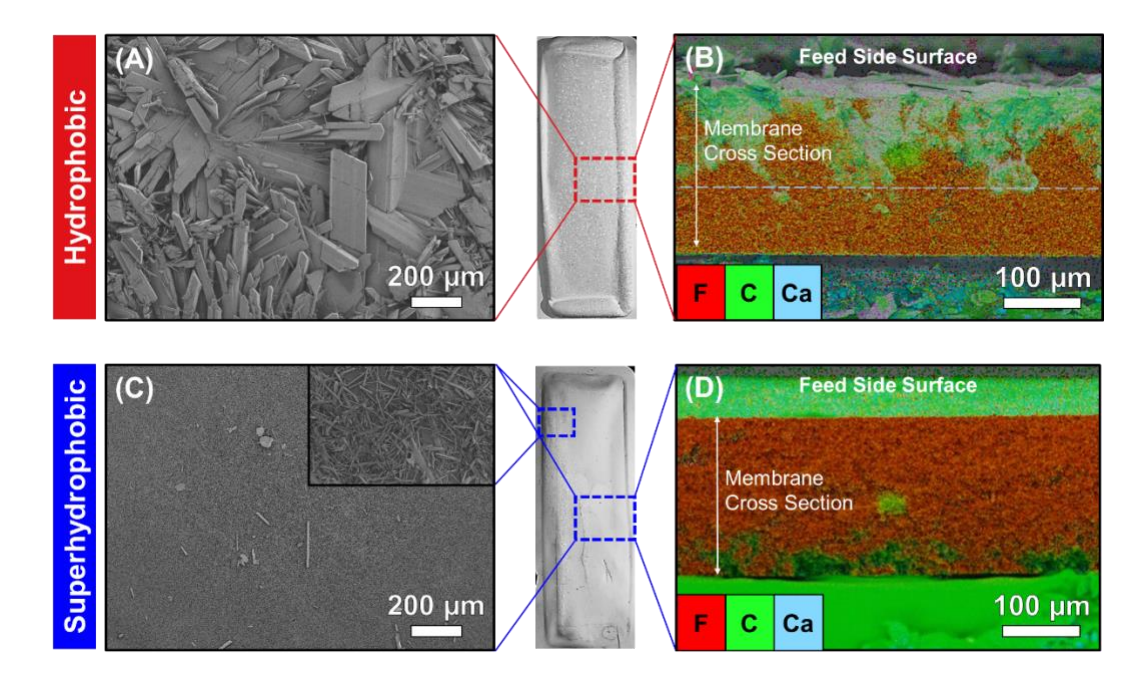


Figure 4: Scale layer characterization on membranes from the MD experiments with purging. Membrane samples were removed from the experimetnal setup and dried immediately after the MD experiments. The photographic images at the center are the same as Figure 3C. (A) top-down SEM image of scale layer on the hydrophobic membrane surface. (B) SEM-EDS map of fluorine (red), carbon (green), and calcium (blue) content in the hydrophobic membrane cross-section. The crystal intrusion depth is approximated by the blue dashed line. (C) top-down SEM images of crystal free region of the superhydrophobic membrane surface (main figure) and the small rod-like crystals along the edge of the superhydrophobic membrane surface (inset). (D) SEM-EDS map of fluorine (red), carbon (green), and calcium (blue) content in the membrane cross section.

Previous studies investigated the use of periodic purging to mitigate scaling in MD with hydrophobic membrane and reported that purging effectiveness was dependent upon the initial feed concentration_{26,27}. For feed solutions with initial concentrations well above saturation, purging was slightly effective in slowing down scaling. At such high initial feed concentrations, a large fraction of the crystals formed in the bulk solution and deposited onto the membrane surface as opposed to growing on the membrane surface via interfacial crystallization. However, for solutions with initial concentrations below saturation (as in the case of this study), purging did not affect the scaling behavior₂₉, which is similar to our experimental observation. These results suggest that purging is more effective at removing crystals that nucleate in the bulk solution and then deposit onto the surface, than removing those that nucleate heterogeneously on the membrane surface

and grow in-situ. As it is less likely to encounter an industrial brine stream with precipitated solid already formed, the use of superhydrophobic membrane that minimizes interfacial crystallization and in-pore growth of crystals is necessary for purging to be effective.

Implications. The proposed novel strategy that synergistically combines membrane superhydrophobicity and physical gas purging has been demonstrated to be highly effective in preventing gypsum scaling in MD. We show that only this synergistic combination, not purging or superhydrophobic membrane alone, can result in truly effective mitigation of membrane scaling. Overcoming the challenge of mineral scaling in MD using this novel strategy will enable MD to treat hypersaline brine with sustainable performance. This strategy can potentially be employed, with additional system integration and innovation, to achieve complete separation of water and salt crystal, and thereby replace mechanical vapor compression as a lower-cost technology using low-grade waste heat for brine concentration and crystallization in ZLD.

284

285

272

273

274

275

276

277

278

279

280

281

282

283

Associated Content

- 286 Illustration of the procedures of fabricating a superhydrophobic via modifying a commercial
- 287 PVDF membrane (Figure S1). Schematic diagram of the experimental setup for membrane
- distillation with purging capability (Figure S2). Distillate conductivity in MD scaling experiments
- 289 (Figure S3).

290 291

Acknowledgements

- 292 This work is partially supported by National Science Foundation via research grant CBET-
- 293 1705048. T.H. acknowledges the support from American Chemical Society Petroleum Research
- Foundation via award ACS-PRF 57353 DNI. C.S. acknowledges the support from China Scholar
- 295 Council via scholarship 201804910753.

296

297

References

- 298 1. Alkhudhiri, A., Darwish, N. & Hilal, N. Membrane distillation: A comprehensive review. 299 Desalination **2012**, 287, 2–18.
- Tong, T. & Elimelech, M. The Global Rise of Zero Liquid Discharge for Wastewater Management: Drivers, Technologies, and Future Directions. *Environ. Sci. Technol.* **2016**, 50, 6846–6855.

- 303 3. Chen, G., Lu, Y., Krantz, W. B., Wang, R. & Fane, A. G. Optimization of operating conditions for a continuous membrane distillation crystallization process with zero salty water discharge. *J. Memb. Sci.* **2014**, 450, 1–11.
- 306 4. Ruiz Salmón, I. & Luis, P. Membrane crystallization via membrane distillation. *Chem.* 307 *Eng. Process. Process Intensif.* **2018**,123, 258–271.
- 5. Creusen, R., Medevoort, J., Roelands, M., Duivenbode, A. R., Hanemaaijer, J. H., Leerdam, R. Integrated membrane distillation-crystallization: Process design and cost estimations for seawater treatment and fluxes of single salt solutions. *Desalination* **2013**, 323, 8–16.
- Edwie, F. & Chung, T. S. Development of simultaneous membrane distillationcrystallization (SMDC) technology for treatment of saturated brine. *Chem. Eng. Sci.* **2013**, 98, 160–172.
- 315 7. El-Bourawi, M. S., Ding, Z., Ma, R. & Khayet, M. A framework for better understanding membrane distillation separation process. *J. Memb. Sci.* **2006**, 285, 4–29.
- 317 8. Deshmukh, A., Boo, C., Karanikola, V., Lin, S., Straub, A. P., Tong, T., Warsinger, D. M., Elimelech, M. Membrane distillation at the water-energy nexus: Limits, opportunities, and challenges. *Energy Environ. Sci.* **2018**, 11, 1177–1196.
- 320 9. Alklaibi, a. M. & Lior, N. Membrane-distillation desalination: Status and potential. 321 Desalination **2005**, 171, 111–131.
- 10. Lin, S., Nejati, S., Boo, C., Hu, Y.,Osuji, C. O., Elimelech, M. Omniphobic Membrane for Robust Membrane Distillation. *Environ. Sci. Technol. Lett.* **2014**,1, 443–447.
- Warsinger, D. M., Swaminathan, J., Guillen-burrieza, E., Arafat, H. A. & V, J. H. L.
 Scaling and fouling in membrane distillation for desalination applications: A review. 2015,
 356, 294–313.
- Shaffer, D. L., Arias Chavez, L. H., Ben-Sasson, M., Castrillon, S. R. V., Yip, N. Y.,
 Elimelech, M. Desalination and reuse of high-salinity shale gas produced water: Drivers,
 technologies, and future directions. *Environ. Sci. Technol.* 2013, 47, 9569–9583.
- Warsinger, D. M., Servi, A., Belleghem, S. V., Gonzalez, J., Swaminathan, J., Kharraz, J.,
 Chung, H. W., Arafat, H. A., Gleason, K. K., Lienhard V, J. H. Combining air recharging
 and membrane superhydrophobicity for fouling prevention in membrane distillation. *J. Memb. Sci.* 2016, 505, 241–252.
- 334 14. Shaffer, D. L., Tousley, M. E. & Elimelech, M. Influence of polyamide membrane surface chemistry on gypsum scaling behavior. *J. Memb. Sci.* **2017**, 525, 249–256.
- Tijing, L. D., Woo, Y. C., Choi, J. S., Lee, S., Kim, S. H., Shon, H. K. Fouling and its control in membrane distillation-A review. *J. Memb. Sci.* **2015**, 475, 215–244.
- Pouget, E., Bomans, P. H. H., Goos, J. A. C. M., Frederik, P. M., de With, G.,
 Sommerdijk, N. A. J. M. The Initial Stages of Template-Controlled CaCO3 Formation
 Revealed by Cryo-TEM. Science 2019, 323, 1455–1458.
- 341 17. Saha, A., Lee, J., Pancera, S. M., Braeu, M. F., Kempter, A., Tripathi, A., Bose, A. New insights into the transformation of calcium sulfate hemihydrate to gypsum using time-resolved cryogenic transmission electron microscopy. *Langmuir* **2012**, 28, 11182–11187.

- Mayer, M., Augustin, W. & Scholl, S. Adhesion of single crystals on modified surfaces in crystallization fouling. *J. Cryst. Growth* **2012**, 361, 152–158.
- 19. Erdemir, D., Lee, A. Y. & Myerson, A. S. Nucleation of Crystals from Solution: Classical
 and Two-Step Models. *Acc. Chem. Res.* 2009, 42, 621-629
- Curcio, E., Fontananova, E., Di Profio, G. & Drioli, E. Influence of the structural properties
 of poly(vinylidene fluoride) membranes on the heterogeneous nucleation rate of protein
 crystals. *J. Phys. Chem. B* 2006,110, 12438–12445.
- 351 21. Karanikola, V., Boo, C., Rolf, J. & Elimelech, M. Engineered Slippery Surface to Mitigate
 352 Gypsum Scaling in Membrane Distillation for Treatment of Hypersaline Industrial
 353 Wastewaters. *Environ. Sci. Technol.* 2018, 52, 14362–14370.
- Xiao, S., Zheng, R., Liu, Y., He, H., Yuan, X., Ji, Y., Li, D., Yin, H., Zhang, Y., Li, X. M.,
 He, T. Slippery for scaling resistance in membrane distillation: a novel porous
 micropillared superhydrophobic surface. *Water Res.* 2019,155, 152–161.
- Razmjou, A., Arifin, E., Dong, G., Mansouri, J. & Chen, V. Superhydrophobic modification of TiO2 nanocomposite PVDF membranes for applications in membrane distillation. *J. Memb. Sci.* **2012**, 415–416, 850–863.
- Zeyu, M., Hong, Y., Liyuan, M. & Su, M. Superhydrophobic membranes with ordered arrays of nanospiked microchannels for water desalination. *Langmuir* **2009**, 25, 5446–5450.
- Xiao, Z., Li, Z., Guo, H., Liu, Y., Wang, Y., Yin, H., Li, X., Song, J., Nghiem, L. D., He, T.
 Scaling mitigation in membrane distillation: From superhydrophobic to slippery.
 Desalination 2019, 466, 36–43.
- Julian, H., Ye, Y., Li, H. & Chen, V. Scaling mitigation in submerged vacuum membrane distillation and crystallization (VMDC) with periodic air-backwash. *J. Memb. Sci.* **2018**, 547, 19–33.
- Zou, T., Dong, X., Kang, G., Zhou, M., Li, M., Cao, Y. Fouling behavior and scaling mitigation strategy of CaSO₄ in submerged vacuum membrane distillation. *Desalination* **2018**, 425, 86–93.
- 372 28. Boo, C., Lee, J. & Elimelech, M. Omniphobic Polyvinylidene Fluoride (PVDF) Membrane 373 for Desalination of Shale Gas Produced Water by Membrane Distillation. *Environ. Sci.* 374 *Technol.* **2016**, 50, 12275–12282.
- Tong, T., Wallace, A. F., Zhao, S. & Wang, Z. Mineral scaling in membrane desalination:
 Mechanisms, mitigation strategies, and feasibility of scaling-resistant membranes. *J. Memb. Sci.* 2019, 579, 52–69.
- 378 30. Nosonovsky, M. & Bhushan, B. Hierarchical roughness optimization for biomimetic superhydrophobic surfaces. *Ultramicroscopy* **2007**,107, 969–979.
- 380 31. Kwon, Y., Patankar, N., Choi, J. & Lee, J. Design of surface hierarchy for extreme hydrophobicity. **2009**, *Langmuir* 25, 6129–6136.
- 382 32. Gryta, M. Calcium sulphate scaling in membrane distillation process. *Chem. Pap.* **2009**, 63, 146–151.
- 384 33. Uchymiak, M., Lyster, E., Glater, J. & Cohen, Y. Kinetics of gypsum crystal growth on a

reverse osmosis membrane. *J. Memb. Sci.* **2008**, 314, 163–172.

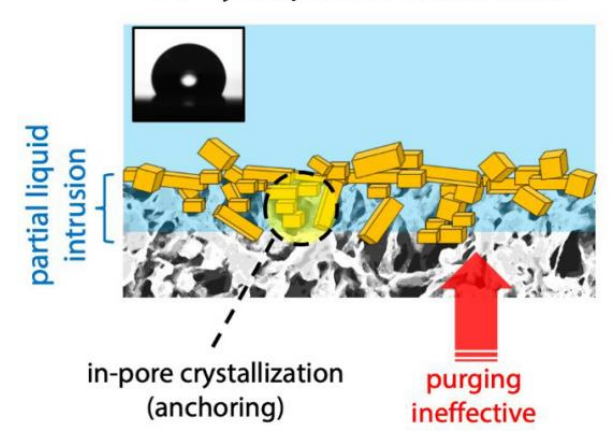
392

- 386 34. Shih, W. Y., Rahardianto, A., Lee, R. W. & Cohen, Y. Morphometric characterization of calcium sulfate dihydrate (gypsum) scale on reverse osmosis membranes. *J. Memb. Sci.* **2005**, 252, 253–263.
- 389 35. Rahardianto, A., Shih, W. Y., Lee, R. W. & Cohen, Y. Diagnostic characterization of gypsum scale formation and control in RO membrane desalination of brackish water. *J. Memb. Sci.* **2006**, 279, 655–668.

393 **Graphical Abstract**

394

(A) Hydrophobic Membrane



(B) **Super**hydrophobic membrane

